Available online at www.sciencedirect.com
ScienceDirect
Engineering Fracture Mechanics 74 (2007) 1054–1078
Engineering Fracture Mechanics
www.elsevier.com/locate/engfracmech

Fracture mechanisms and fracture toughness in semicrystalline polymer nanocomposites

B. Cotterell *, J.Y.H. Chia, K. Hbaieb

Institute of Materials Research and Engineering, 3 Research Link, Singapore 117602, Singapore

Available online 27 December 2006

Abstract

Polymer nanocomposites, especially nanoclay composites, have received much attention in recent years. While it is the functional properties of these composites that are the driving force, good mechanical properties are necessary in most applications. Although claims are made that the mechanical properties of nanocomposites should be excellent, in practice the mechanical properties are often disappointing. Soft or hard spherical particles can toughen semicrystalline polymers, but plate-like nanoclay particles have not produced any significant toughening action and frequently cause significant embrittlement. In this paper the toughening of semicrystalline polymers with nanoparticles, and particularly the difference in behaviour of spherical and plate-like particles is reviewed.

Keywords: Semicrystalline polymers; Nanocomposites; Spherical particles; Nanoclay particles; Toughness

1. Introduction

For the last ten years or so there has been considerable interest in polymer nanocomposites and in particular nanoclay composites and Tjong [1] has recently given a comprehensive review. Functional properties such as fire and moisture permeability resistance [2,3] and some specific mechanical properties such as creep and wear resistance [4,5] are the driving forces for the development of polymer nanocomposites. However, nanocomposites need sufficient stiffness, strength and toughness for their particular design purpose. Stiffness is improved by high modulus particles of any size or shape, though there may be secondary stiffening effects in semicrystalline polymers from the effect of the particles on the lamellar crystal growth [6]. Strength and toughness are very much interlinked, with toughness usually being more important than strength. Soft or hard particles of a wide range of shape and size can toughen glassy polymers [7]. In semicrystalline polymer nanocomposites while soft and hard near spherical particles can, in the right size volume combination, increase the toughness, high aspect ratio clay platelets in general do not significantly toughen the polymer and in many cases cause significant embrittlement. It is the purpose of this paper to review the toughness of semicrystalline

* Corresponding author.
E-mail address: brian-c@imre.a-star.edu.sg (B. Cotterell).

0013-7944/$ - see front matter © 2006 Published by Elsevier Ltd.
doi:10.1016/j.engfracmech.2006.12.023

polymer nanocomposites and to suggest reasons why the shape of the particles is so important in determining the toughness.

1.1. Characterisation of toughness

The processing of polymer nanocomposites is generally difficult. There are problems with the agglomeration of nanoparticles and dispersing agents are often needed [1]. Clay nanoparticles need modification to enable intercalation or exfoliation of the particles. Coupling agents are frequently used to promote bonding of the polymer to the particles [8]. Thus the development of polymer nanocomposites has largely been the province of chemists and the physical characterisation of the nanocomposites, such as wide angle X-ray scattering (WAXS) to determine silicate interlayer distances, has generally received more thought than mechanical characterisation. In the case of the simpler mechanical properties such as Young's modulus or yield strength[1] the testing techniques are simple and require little thought or interpretation. However, toughness is a more difficult property to characterise.

The more brittle polymer nanocomposites can be characterised by the plane strain fracture toughness, K_{Ic}, obtained from well established linear elastic fracture mechanics [9,10], though even here due attention is not always made to obtain valid K_{Ic} values, especially in regards to the specimen size, which is often minimised because the nanocomposites are usually only produced in quite small volumes. However, provided the standard test methods are strictly followed there is no real difficulty in obtaining valid plane strain fracture toughness values.

Characterisation of the toughness of the more ductile semicrystalline polymer nanocomposites can provide more of a challenge, which is due to the relatively tougher matrix and also due to the injection moulding process used to produce fracture specimens where the flow conditions near the gate are different to those at the far end. Traditionally toughness has been characterised by the Izod or Charpy impact energy. It has long been recognized that the impact energy is a very complicated strain rate function of the plastic and fracture work with generally the plastic work dominating. The Izod and Charpy tests have lost favour in mechanical engineering because they cannot be used directly in design, but they still have use for comparing the toughness of a particular polymer nanocomposite system. In their desire to characterise toughness of ductile polymer nanocomposites more exactly, many researchers have turned to fracture mechanics. It is generally appreciated that fracture initiation at high stress cannot be explained by linear elastic fracture mechanics. However, the post yield fracture mechanics J-integral approach [11], used by many to characterise the toughness of ductile polymer nanocomposites, has many limitations. These limitations were first discussed in relation to the ductile fracture of metals, but apply equally to polymers. Unless the fracture process zone is very small the value of the J-integral at initiation, J_{Ic}, depends upon the degree of constraint at the crack tip, which is a function of geometry and size, especially specimen thickness [12].[2] More importantly ductile semicrystalline polymers and their nanocomposites often exhibit considerable crack growth resistance before the fracture becomes unstable. This crack growth resistance can often be seen visually from the fractured specimens where the quasi-plane strain conditions prevailing at the notch inhibit contraction in thickness which increases with crack growth [14]. Attention is not always paid to the conditions for validity, especially on thickness, and some crack growth resistance is due to this plane strain/plane stress transition. Crack growth resistance is known to be size and geometry dependent for other than very small crack extensions [15–17]. If there is significant crack growth resistance, J_{Ic} is not a good measure of the toughness of a nanocomposites. The crack growth resistance as characterised by J_R, though being size and geometry dependent is a better comparative measure of the toughness for specimens of the same geometry and size than is the initiation J_{Ic}. Side grooved specimens, which would eliminate some of the crack growth resistance due to a plane stress–plane strain transition, by

[1] In this paper the term yield strength or stress will be used to mean the limit of elastic deformation not the stress at instability in a tension test as is usually the case in the polymer community.

[2] Apart from the effect of thickness on toughness there is an equal if not more important thickness effect in injection moulded specimen where there is a skin effect. Uribe-Arocha et al. [13] has shown that the thin nylon 6 clay nanocomposite tensile specimens are stiffer and fracture in a more brittle fashion than thick ones.

providing constraint induced plane strain, are unfortunately not usual. The initial crack growth resistance is usually linear in the crack growth, a, and the stability of fractures in ductile materials can be judged from the non-dimensional tearing modulus

$$T = \frac{E}{\sigma_Y^2}\frac{dJ_R}{da} \tag{1}$$

where E is Young's modulus, σ_Y, is the yield strength; fracture is stable if the tearing modulus is greater than a non-dimensional function of the specimen geometry [18].

The J-integral approach is a natural extension of linear elastic fracture mechanics and works best for not too ductile fractures. An alternative approach that works best for very ductile fracture that has been used for polymer nanocomposites [19–22] is the essential work of fracture (EWF) approach. This approach was first proposed for plane stress ductile metal fractures [23] and later applied to polymers [24]. The aim of the EWF approach is to separate the work performed in the fracture process zone (FPZ) from the total work of fracture that in ductile polymers is often dominated by the work of plastic deformation. The work performed in the FPZ, termed the essential work of fracture, is a quasi-material property only dependent on the specimen thickness. The EWF method makes use of the fact that the essential work and the plastic work scale differently. If the entire specimen ligament deforms plastically before fracture initiation then the specific essential work can be found by testing different ligament lengths and extrapolating the specific total work of fracture to zero ligament length. In recent years the EWF method has been extensively applied to polymers and is a draft standard of the European Structural Integrity Society (ESIS) [25]. The EWF approach can also be used for plane strain fracture J_{Ic} either obtained from slow strain rate tests [26,27] or impact tests [28]. The EWF method is not without its difficulties: it needs multiple specimens, the limits for valid ligaments are difficult to set precisely and there is some difficulty in getting repeatable results from different laboratories [25,29], but it does deliver a single fracture parameter that is representative of crack propagation.

Since the methods used to characterise the fracture toughness of semicrystalline polymer nanocomposites are so varied, it is likely that some of the differences in fracture toughness reported for nanocomposites come from the difference in the methods of characterisation rather than real differences in the material.

1.2. Toughness of semicrystalline polymer nanocomposites

There is a tendency to believe that the all the properties of composites must be enhanced if the particle size is very small. Small particle size has a positive effect on many of the functional properties of polymer composites. The direct effect on stiffness of particles is neutral in regards to particle size. Toughness is particle size dependent. There are many toughening mechanisms in composites which cannot be effective with nanoparticles. For example nanoparticles are too small to cause significant crack bridging or crack deflection. On the other hand the very large surface area of nanoparticles does provide the possibility of large energy absorption if they delaminate. However, even here there is an optimum particle size for toughening because the stress necessary to cause delamination is inversely proportional to the square root of the particle size. Rubber particles have long been used to toughen polymers. The particles cavitate and promote shear yielding or multiple crazing [30]. Wu [31] showed that for nylon 6.6 that significant toughening occurred when the inter particle spacing was less than a critical distance and went on to conclude that this was the most basic factor in rubber toughening of polymers in general, but also added an important proviso that the particles must not be too small or they cannot cavitate [32]. The critical interparticle toughness concept is appealing, but has not been universally accepted. It has also been long understood that a similar toughening action can be obtained with rigid as well as soft particles provided they delaminate reasonably easily [33]. The only difference between the cavitation of a rubber particle and the debonding of a rigid particle is that the rigid particle prevents Poisson's contraction of the void. Spherical nanosized rigid particles, particularly $CaCO_3$ particles, can be an effective method of toughening semicrystalline polymers [14,34–38]. However, semicrystalline polymers are not significantly toughened and in most cases very significantly embrittled by nanoclay particles [20,22,39–45].

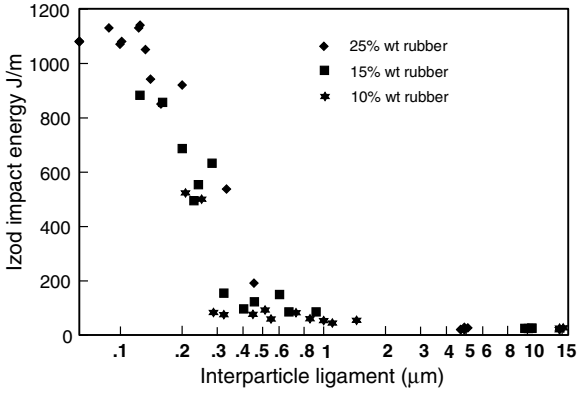

Fig. 1. Izod energy for nylon 6.6 reinforced with a hydrocarbon rubber with a strong adhesion to the nylon for particle sizes from 0.32 to 2.32 μm and weight fractions from 10% to 25% as a function of the interparticle ligament distance; after Wu [31].

2. Semicrystalline polymers reinforced by spherical particles

The existence of a critical interparticle ligament distance, $\Lambda_c = 300$ nm, for the toughening of nylon 6.6 by rubber particles first demonstrated by Wu [31] and his much quoted data is shown in Fig. 1. Muratoglu et al. [46] obtained similar results for nylon 6 and gave the critical interparticle ligament size as between 300 and 500 nm.

High density polyethylene (HDPE) was shown to be toughened by rubber particles provided the interparticle ligaments were less than 600 nm [47]. The same critical interparticle ligament distance, $\Lambda_c = 600$ nm, was found for toughening of HDPE by $CaCO_3$ particles [38]. However, Lazzeri et al. [48] found that 10% volume fraction of stearic acid treated precipitated $CaCO_3$ with an average diameter of 64 nm embrittled HDPE[3] even though the interparticle ligament was only about 50 nm.

The critical interparticle ligament concept does not completely explain the toughness of polypropylene nanocomposites. Thio et al. [35] measured the impact resistance of isotactic polypropylene (iPP) toughened with three sizes of $CaCO_3$ particles with nominal mean particle diameters of 3.5, 0.7 and 0.07 μm. With volume fractions up to 30% they found that only the 0.7 μm particles produced any significant increase in impact energy and stated that "based on these observations, the mechanism of toughening appears to be unrelated to the interparticle distance". However, there were other reasons why the 3.5 and 0.07 μm particles did not toughen. The smallest particles agglomerated and contained a significant number of agglomerations 47–56 μm in size and the largest particles were irregular in shape and size. Large particles or agglomerations can form fracture initiation sites and it only requires one near the notch to cause premature fracture. Thio et al. [35] also measured J_{Ic}, albeit by an indirect non-standard method, which did show a significant increase at 10% volume fraction but decreased markedly at higher volume fractions for all particle sizes. However, the initiation J-integral is not a good measure of toughness because both pure and reinforced PP shows a considerable crack growth resistance [34] and the work of Thio et al. [35] does not by itself disprove the critical interparticle ligament concept. Zuiderduin et al. [36] also examined iPP/$CaCO_3$ nanocomposites with an average particle size of 0.7 μm and a narrow size distribution. The particles were stearic acid treated. The Izod toughness increased linearly with particle volume fraction up to the maximum volume fraction of about 34%. At the highest particle volume fraction the toughness was about four times that of the unfilled iPP which agrees closely with the results of Thio et al. [35] for their results with nominally 0.7 μm particles. Zhang et al. [37] have also measured the impact resistance of iPP/CaO_3 (without the use of any additive) with an average particle diameter of 44 nm. and achieved roughly comparable results to those of Thio et al. [35] and Zuiderduin et al. [36] except at their highest particle volume fraction of 8.6% where the toughness dropped sharply.

[3] There was agglomeration of the particles with low stearic acid concentrations, but even at the highest concentrations, where there was little agglomeration, the impact energy was still less than that of unfilled HDPE.

A non-ionic modifier, polyoxyethylene nonphenol (PN), in various amounts was also used on particles with a volume fraction of 6.23% by Zhang et al. [37]. The PN modifier gives better dispersion of the particles, but also increases the β-phase in the iPP and decreases the adhesion between the particles and the iPP. The PN modifier increased the Izod impact energy of the 6.23% volume fraction nanocomposites from about 28 to 45 J/m, which is comparable to the Izod impact energies obtained by Thio et al. [35] at the higher volume fraction of 23.3%.

One of the problems in assessing the effect of $CaCO_3$ particles on the toughness of iPP nanocomposites is that the particles and additives can change the crystalline structure and toughness of the matrix. There are three forms of iPP: α-phase, the most common, β-phase, a metastable phase, and γ-phase. Particles form ready nucleation sites for the β-phase. Additives such as stearic acid and PN modifier promote the β-phase. The β-phase can also be induced by allowing crystallization to take place at elevated temperature. Labour et al. [50] have studied the effect of the β-phase on the toughness of both unfilled and filled iPP. They observed considerable crack growth resistance and characterised the toughness with $J_R$curves which are shown in Fig. 2 for both unfilled and filled iPP with 10% wt fraction of stearic acid treated $CaCO_3$ particles of average diameter 100 nm. Here the toughness of these unfilled and filled iPP has been arbitrarily defined as the J_R for a crack growth of 1 mm and the normalized results are shown as a function of the β-phase percentage, defined as $100\beta/(\alpha+\beta)$, in Fig. 3; assuming a cubic array, the interparticle distance is 135 nm. Also shown in Fig. 3 are the Izod impact results for Zhang et al. [37] for 15% weight fraction of 440 nm $CaCO_3$particles; the interparticle distance for these nanocomposites is 45 nm. The β-phase significantly increases the toughness of the

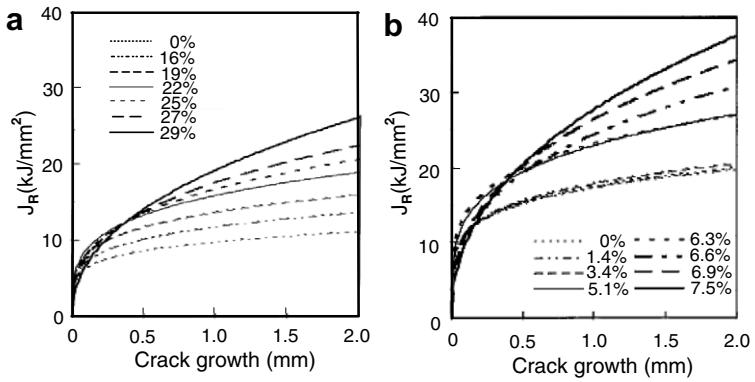

Fig. 2. J_R curves for (a) unfilled and (b) filled iPP for various β-phase contents; after Labour [50].

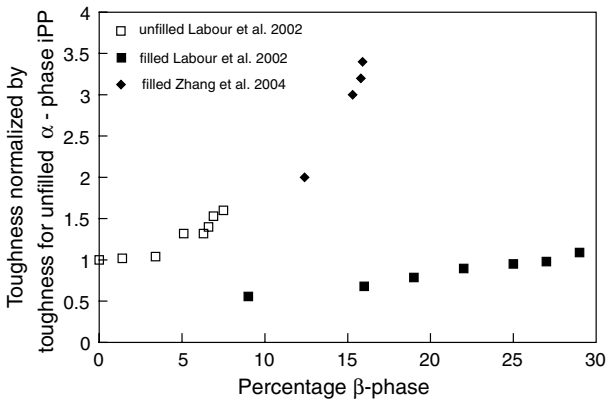

Fig. 3. Toughness of filled and unfilled iPP normalized by the toughness of unfilled α-phase iPP as a function of the β-phase percentage for results of Labour et al. [50], and Zhang et al. [37].

unfilled iPP. The β-phase has significantly lower yield strength than the α-phase and consequently the β-phase spherulites are more highly strained than the α-phase ones and more readily craze [50,51]. It is multiple crazing that is a major energy absorption mechanism in semicrystalline polymer nanocomposites. Even without isothermal crystallization at elevated temperature the stearic acid treated particles cause a significant β-phase in the filled iPP, but the toughness of the nanocomposites of Labour et al. [50] is less than the toughness of the unfilled α-phase iPP except for the highest concentrations of the β-phase. The interparticle distance for the Labour et al. [50] nanocomposites is very much larger than the nanocomposites of Zhang et al. [37] presented in Fig. 3. Labour et al. [50] do not report agglomeration of their particles and the 100 nm particles are unlikely to cause premature fracture initiation, and the reason for the embrittlement is not clear. The nanocomposites of Zhang et al. [37] which have a much smaller interparticle ligament (45 nm) are very significantly tougher than the unfilled α-phase iPP. The $CaCO_3$ particles used by Zhang et al. [37] were treated with a different modifier to improve dispersion and were injection moulded after compounding by melt extrusion whereas Labour et al. [50] used compression moulding to produce the samples. However, these differences are unlikely to account for the big difference in toughness behaviour. The most likely cause of the difference is the difference in the interparticle ligaments.

Perhaps the strongest evidence against the critical interparticle ligament concept comes from the recent work of Corté et al. [52] who performed Charpy impact tests on nylon 12 containing two types of rubber particles, ethylene/propylene (EPR) and poly-(styrene)-block-poly(methyl methacrylate) triblock terpolymer (SBM), both as injection moulded and after re-melting in a mould at 200 °C and very slowly cooling. Their results are shown in Fig. 4. For the as-injection moulded specimens the critical interparticle ligament size is somewhere between 1.2 and 2.0 μm, but for the re-melted and slowly cooled specimens the transition to ductile behaviour clearly occurs at a much smaller ligament size of 500–600 nm. Since the slow cooling produces a different crystalline structure, which will be discussed in Section 2.1, it could be argued that in effect there are two different matrix materials and so the evidence of Corté et al. [52] does not completely disprove Wu's criterion. A similar comment could be made for the iPP specimens though then it is necessary to compare specimens with similar β-phase contents. Assuming that the toughness for the unfilled iPP with 9% β-phase is not far different to that at 7.5%, which was the highest β-phase content in the experiments of Labour et al. [50], then the toughness of iPP with 10% weight fraction of $CaCO_3$particles and a matrix containing 9% β-phase relative to the unfilled iPP of similar β-phase content would be only 0.35, which represents a very marked embrittlement. It is not so easy to do the same comparison for the results of Zhang et al. [37] but, judging from the toughening effect of the β-phase on the unfilled iPP shown by Labour et al. [50], the nanocomposite with the 15% weight fraction of unmodified $CaCO_3$ particles is embrittled relative to an unfilled specimen of the same β-phase content.

It is clear that there are many factors which affect the toughness of semicrystalline polymers reinforced with hard particles. Interparticle ligament size appears to be possibly one. However, there are many other factors

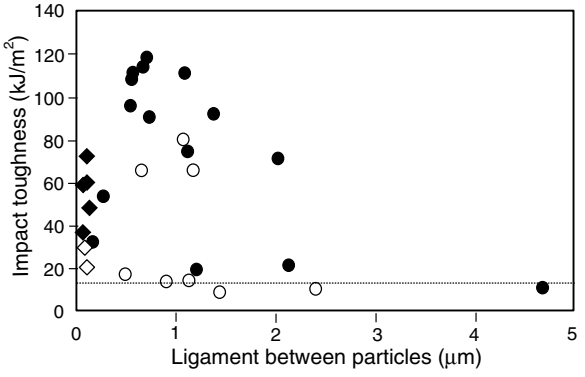

Fig. 4. Charpy impact toughness as a function of the average interparticle ligament. Full symbols are for as injection moulded samples and open symbols for re-melted and slowly cooled specimens (●, ○ SBM particles; ♦, ◇ EPR particles). The horizontal dotted line represents the impact energy for unfilled nylon 12; after Corte et al. [52].

involved. The effect of the particles and dispersants on the crystal structure is very important and can have a major effect on the toughness of iPP. Other factors are discussed below.

2.1. Crystalline orientation and the critical ligament concept

The critical interparticle ligament concept is not in itself a toughness mechanism, but only the possible consequence of a mechanism. In an attempt to understand the concept physically the critical ligament concept has been linked to transcrystallinity. Muratoglu et al. [46] spun coated thin films of nylon 6 containing rubber particles on polystyrene, which was later dissolved. Staining the thin films with phosphotungstic acid they revealed that around the rubber particles the lamellar crystals were orientated normal to the rubber surface, but were not able to measure the extent of the orientation. To examine the transcrystallization further Muratoglu et al. [53] examined the crystalline morphology of thin films sandwiched both between a rubber and polystyrene. When the nylon film was thinner than 150 nm, the lamellar crystallites were found to be orientated so that the *c*-axis of the lamellae was parallel to the surface of the rubber or polystyrene.

Bartczak et al. [54] repeated the experiments of Muratoglu et al. [53] with thin films of HDPE sandwiched between rubber and calcite surfaces. They found that the lamellae were orientated for films less than 400 nm. These experiments seem to indicate that the critical interparticle ligament can be identified with a transcrystallized layer existing around particles with the lamellae orientated normal to the surface. Normally a transcrystalline layer only grows epitaxially from a crystalline surface, but a transcrystalline layer can be obtained by shearing the melt on amorphous surfaces [55]. The group at the Caseli Institute examined lamellar growth, in nylon 66 from carbon and armid fibres and in HDPE from ultra high molecular weight polyethylene fibres, in all cases they found the lamellae grew radially from the fibre for distances up to 20 μm; in the case of polyethylene they found that they were twisted in to a helix [55–57]. Kim et al. [58] have also shown lamellae that have grown normal to synthetic silicate layers spaced about 200 nm apart in nylon 12 (see Fig. 5).

Corté et al. [52] examined the crystal structure of stained ultra thin sections cut by ultramicrotomy from nylon 12 composites described in Section 2.1. The TEM microphotographs are shown in Fig. 6. The orientation of the lamellae in the as injection moulded samples (see Fig. 6a and b) does not seem to be affected by the rubber particles and is normal to the injection moulded direction, that is in the direction of cooling. Likewise in the slowly cooled recrystallized samples the lamellae orientation does not seem to be affected by the rubber particles, but their orientation is arranged in ''grains''. Corté et al. [52] criticize the work of Muratoglu et al. [53] since it was performed with thin spun coated films rather than bulk nanocomposites. In the case of the evidence of Kim et al. [58] the silicate layers are aligned in the injection moulding direction and so are both normal to the moulding direction as well as normal to the silicate layers. The size of the orientated lamellae zone observed on fibres [55–57] is so large that it cannot be used as evidence of the much smaller orientated

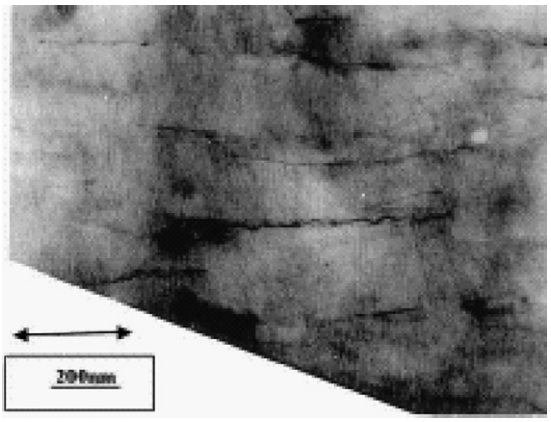

Fig. 5. TEM of nylon 12 synthetic layer silicate nanocomposite showing lamellae aligned normal to the silicate layers; from Kim [58].

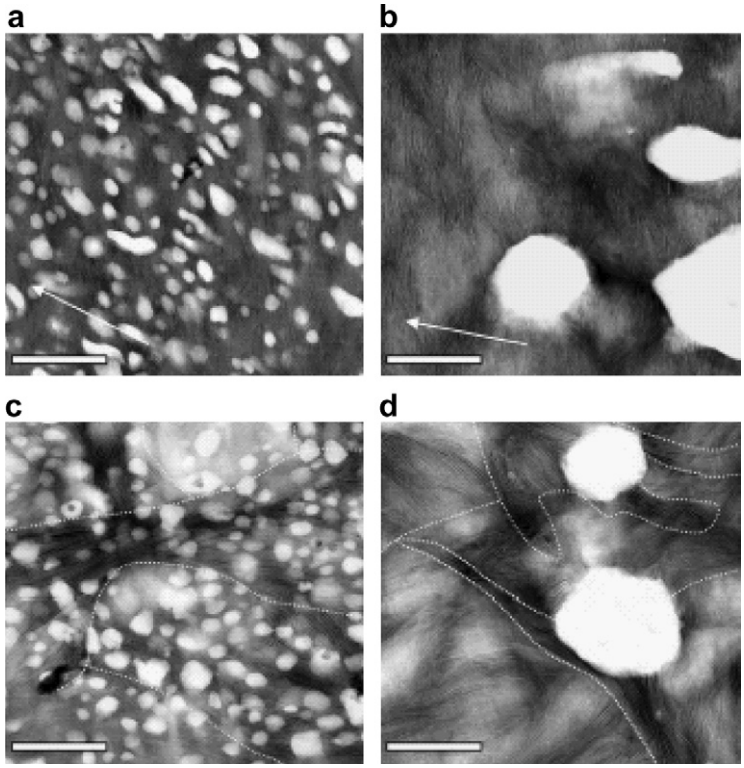

Fig. 6. TEM micrographs of strained ultramicrotomed sections of rubber reinforced nylon 12. The staining shows the crystalline lamellae (bright) areas and the amorphous layers (dark); the unstained rubber particles are bright. As injection moulded samples (a) 20% EPR particles, (b) 15% SBM particles; the arrows show the injection moulded direction. Recrystallized samples (c) 20% EPR particles, (d) 15% SBM particles; white dotted lines outline "grain boundaries". Scale bars = 500 nm; from Corte et al. [52].

zones that are proposed to exist on nanoparticles. Hence there seems no conclusive evidence whether lamellae orientate themselves normal to nanoparticle surfaces.

2.2. Hard particle delamination

There is general consensus that to obtain high toughness particles must cavitate or delaminate at about the constrained yield stress. Evidence of delamination can sometimes cause a distinct change in slope in the elastic part of a tensile stress–strain curve as observed by Wilbrink et al. [14] for nylon 6/$CaCO_3$ nanocomposites. A necessary condition for complete delamination is that the energy released by the delamination is equal to or greater than the delamination toughness of the particle surfaces. Here delamination is examined at the constrained yield stress and so the deformation is essentially elastic. Near the tip of a crack the elastic stress is near hydrostatic and so delamination under a pure hydrostatic stress is considered. First a very dilute composite is considered which can be modelled as a single spherical particle in an infinite solid under a hydrostatic stress σ_h. The stress distribution for the matrix is given by [59]

$$\begin{aligned}\sigma_r &= \sigma_h\left[1-\left(\frac{a}{r}\right)^3\right]+\sigma_i\left(\frac{a}{r}\right)^3\\ \sigma_t &= \sigma_h\left[1+\frac{1}{2}\left(\frac{a}{r}\right)^3\right]+\frac{\sigma_i}{2}\left(\frac{a}{r}\right)^3\end{aligned} \tag{2}$$

where σ_r and σ_t are the radial and tangential stresses, σ_i is the radial stress at the interface of the particle and matrix and a is the radius of the particle. Assuming that there are no residual stresses, the interface stress can be found by the condition of continuity at the interface and is given by

$$\sigma_i = \frac{3\sigma_h(1-\nu_m)}{2(1-2\nu_p)\frac{E_m}{E_p}+(1+\nu_m)} \tag{3}$$

where E_m and E_p are the Young's moduli of the matrix and particle, and ν_m and ν_p are the Poisson's ratio of the matrix and particle. If the particle debonds at constant hydrostatic stress work is done by the hydrostatic stress and the strain energy increases. The net release of energy can be calculated to be

$$W = \frac{9\pi}{8}\left(\frac{\sigma_h^2 d^3}{E_m}\right)\frac{(1-\nu_m)^2}{\left[(1+\nu_m)+2(1-2\nu_p)\frac{E_m}{E_p}\right]} \tag{4}$$

where $d = 2a$ is the diameter of the particle. If Γ_d is the delamination toughness (twice the surface energy) then it is possible for the particle to delaminate if

$$\Gamma_d \leqslant \frac{9}{8}\left(\frac{\sigma_h^2 d}{E_m}\right)\frac{(1-\nu_m)^2}{\left[(1+\nu_m)+2(1-2\nu_p)\frac{E_m}{E_p}\right]} \tag{5}$$

The larger the particle the easier is delamination, but too large a particle can cause premature fracture initiation. Taking for example a dilute PP/$CaCO_3$ nanocomposite assuming $E_m = 1.4$ GPa, $\nu_m = 0.35$; $E_p = 26$ GPa, $\nu_p = 0.2$, complete delamination is possible if

$$\left(\frac{\sigma_h^2 d}{E_m}\right) > 3\Gamma_d \tag{6}$$

For non-dilute nanocomposites with a particle volume fraction v_p the increase in strain energy per unit volume of the composite due to delamination of all the particles is given by

$$\Delta U = \frac{\sigma_h^2}{2E_m}\left[\frac{1}{K_v}-\frac{1}{K_p}\right] \tag{7}$$

where K_p is the bulk modulus of the fully bonded nanocomposite and K_v is the bulk modulus of the nanocomposite with the particles replaced by voids. The net energy released by delamination is numerically equal to the increase in strain energy. The total surface area, S, of the particles per unit volume of the nanocomposite is

$$S = \frac{6v_p}{d} \tag{8}$$

and hence delamination is possible if

$$\Gamma_d \leqslant \frac{1}{12v_p}\left(\frac{\sigma_h^2 d}{E_m}\right)\left[\frac{E_m}{K_v}-\frac{E_m}{K_p}\right] \tag{9}$$

The bulk moduli K_p and K_v can be calculated from the Mori and Tanaka [60] model using the results of Wang and Pyrz [61]. Taking a PP/$CaCO_3$ nanocomposite and using the parameters given above the non-dimensional critical particle diameter $\bar{d} = d/(E_m\Gamma_d/\sigma_h^2)$ can be calculated as a function of the volume fraction of the particles and is shown in Fig. 7. The critical diameter is only a very weak function of the volume fraction and Eq. (6) is accurate enough for practical applications. Zhang et al. [37] using a PP/$CaCO_3$ nanocomposite with an average particle diameter of 44 nm found a significant increase in Izod strength for a volume fraction of about 6%. The yield strength of PP is about 20 MPa, assuming that the constrained yield strength is three times the uniaxial yield strength[4] and the Young's modulus of PP is 1.4 GPa, Eq. (6) predicts than delamination will occur at about the constrained yield strength if the delamination toughness is less than 40 mJ/m^2, which is a very small toughness. The surface energy of $CaCO_3$ is about 200 mJ/m^2, but stearic acid treatment can reduce the surface energy to 40–50 mJ/m^2 [62]. Zhang et al. [37] found that the use of the PN modifier, which as well as increasing the percentage of β-phase crystals also decreased the surface energy, increased

[4] Slip line theory gives the maximum stress ahead of a crack tip as $(2+\pi)\sigma_Y/\sqrt{3} \approx 3\sigma_Y$ and the hydrostatic stress as $(1+\pi)\sigma_Y/\sqrt{3} \approx 2.4\sigma_Y$ [63].

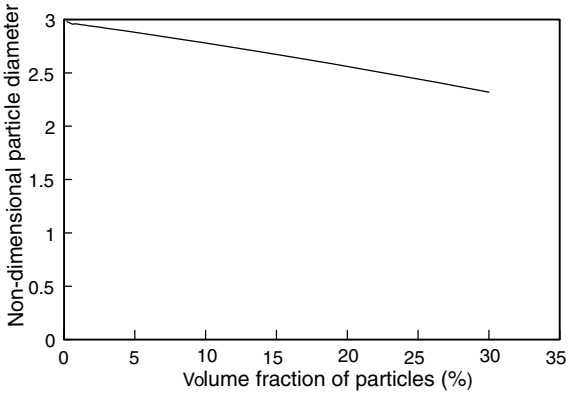

Fig. 7. Non-dimensional critical particle diameter for delamination at a hydrostatic stress σ_h for PP/$CaCO_3$ ($E_m = 1.4$ GPa, $v_m = 0.35$; $E_p = 26$ GPa, $v_p = 0.2$) as a function of particle volume fraction.

the impact energy significantly. In view of the very low toughness predicted for delamination at about the constrained yield stress, it seems likely that a significant portion of the increase in toughness observed by Zhang et al. [37] must have come from earlier delamination of the particles.

2.3. The contribution to toughness of nanocomposites from the delamination of spherical particles

An estimate of the significance of the energy absorbed by particle delamination can be obtained from linear elastic fracture mechanics (LEFM), even though the fracture of semicrystalline polymer nanocomposites cannot be accurately modelled this way. Using LEFM, the maximum hydrostatic stress near the tip of a fracture is given by

$$\sigma_h \approx \frac{0.8K_{Ic}}{\sqrt{2\pi D}} \tag{10}$$

where $K_{Ic} = \sqrt{\Gamma_c E_c}$ is the fracture toughness of the nanocomposite, Γ_c is the fracture energy of the nanocomposite, E_c, and D is the maximum width on either side of the fracture plane that obtains the hydrostatic stress, σ_h. The number of particles per unit area of fracture plane is given by

$$N = \frac{12 v_p D}{\pi d^3} \tag{11}$$

where v_p is the volume fraction of the particles, and the maximum contribution to the fracture toughness, Γ_{del}, that can come from particle delamination is given by

$$\Gamma_{del} = N\Gamma_d \pi d^2 = 12 v_p \Gamma_d \frac{D}{d} \tag{12}$$

Substituting for Γ_d from Eqs. (6) and (10) assuming $E_c \approx E_m$ yields

$$\frac{\Gamma_{del}}{\Gamma_c} \approx 0.4 v_p \tag{13}$$

Thus the contribution of the energy of the delamination of particles is only dependent on the volume fracture and does not depend on the particle size. For a 20% volume fraction of particles, the maximum contribution to the fracture energy is only about 8%. Thus it can be concluded that the energy absorbed in delamination of spherical particles is only a very minor part of the fracture toughness of composites with spherical nanoparticles.

2.4. Matrix energy absorbing mechanisms

The toughness of nanocomposites comes mainly from the energy absorbed in fracturing the polymer matrix, through shear yielding between particles without dilatation, and the formation of multiple craze-like

bands with dilatation. For the latter mechanism to occur the particles must first cavitate or delaminate which absorbs energy. During shear yielding the plastic deformation is concentrated in shear bands where the strain is high enough to cause strain softening. On further straining the shear band hardens as the polymer molecules become orientated causing further shear bands to be nucleated. Under crossed polarizers shear yielding shows up as a zone of birefringence where the polymer has been orientated due to the deformation. Craze-like bands can be either true crazes or dilatational bands. In true crazes the craze nucleates at voided particles; microvoids are created and the ligaments between microvoids then draw out creating stable thin fibrils of highly orientated polymer. The other craze-like band, which has been identified more recently, is the dilatational band where the deformation is akin to the deformation at the tip of a crack in a ductile metal [64]. The voided particles grow under hydrostatic stress causing strain softening because of the reduction in the ligament spacing. Often it is difficult to distinguish between true crazes where initiation and growth of voids in the ligaments is the most important feature and dilatational bands where it is the growth of voided particles that is the most important feature and so they are often described collectively as craze-like bands. The main toughening mechanism in semicrystalline polymers reinforced by spherical nanoparticles is multiple craze-like banding.

The fracture behaviour of notched semicrystalline polymer and their nanocomposites depend upon whether single or multiple crazes are formed. The first stage in craze initiation is the formation of microvoids. Crazes then form by local drawing of the ligaments between the microvoids to form highly orientated fibrils. As the tip of the craze advances the craze widens primarily by drawing material into the craze from its edge. This drawing of material into the craze is a rate controlled process. The fibrils do harden as they stretch and the stress-craze opening curve depends upon the relative ease of drawing the material into the craze to the compliance of the fibrils [65]. The stress-craze opening behaviour is shown schematically in Fig. 8 and can represent strain softening if it is relatively easy to draw material into the craze or strain hardening if it is relatively difficult. Under strain softening, the material adjacent to the craze unloads with further strain and it is not possible to initiate more crazes and a single craze forms. However, if the craze strain hardens then the stress adjacent to the craze increases with further strain and more crazes can be initiated leading to multiple crazing.

Craze-like bands are seen in the optical micrographs of iPP/rubber nanocomposite specimens deformed to near the point of fracture shown in Fig. 9 [66]. In the bright field micrographs craze-like bands can be seen growing from the notch tip (Fig. 9a and c). Under crossed polarizers there is significant birefringence suggesting that there is also shear yielding (Fig. 9b and d). SEM micrographs at higher magnification show the craze-like bands to be dilatational bands (Fig. 10). With 20% weight fraction the nanocomposite of Zebarjad et al. [66] achieved about twice the Charpy impact energy as the unfilled iPP. Fasce et al. [67] used double notch specimens to study the deformation mechanisms in iPP with elastomeric polyolefin (POE) particles under slow and high strain rates. The specimens were compression moulded annealed at 120 °C and slowly cooled. In contrast to injection moulded specimens, which only have a small spherulitic core, these specimens are spherulitic. They observed craze-like bands which increased in density with increase in the POE content, though the bands at high strain rate were more diffuse. The crazes were both trans and inter spherulitic for both low and high

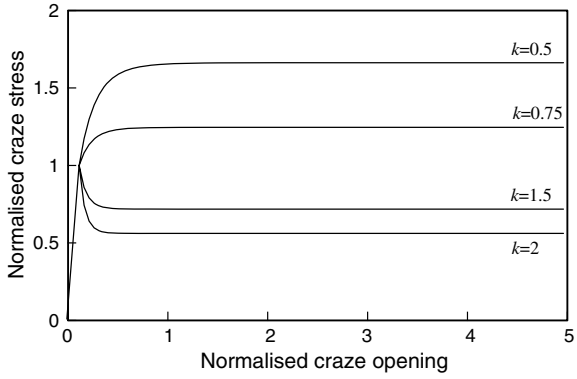

Fig. 8. The stress-craze opening relationship, k is the ratio of craze widening by drawing to craze opening by fibril stretching; after Estevez et al. [65].

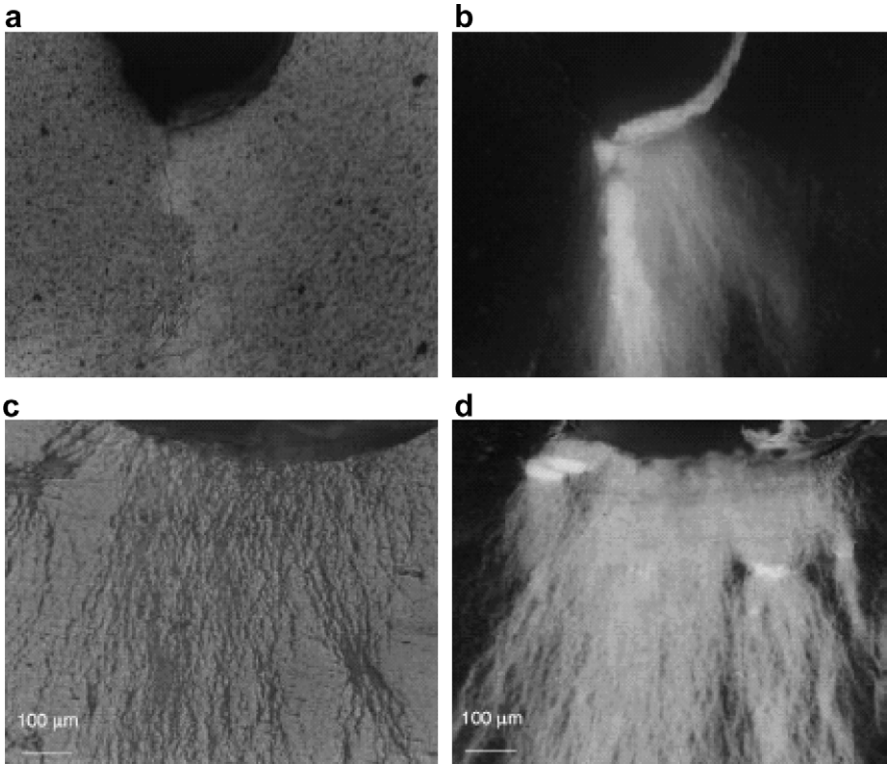

Fig. 9. Optical micrographs of polished surfaces of 3-point bend specimens after deformation in three-point bending test. (a) Craze-like bands at limited deformation (bright field). (b) Craze-like bands at limited deformation (dark field). (c) Craze-like bands at further deformation (bright field). (d) Craze-like bands at further deformation (dark field); from Zebarjad et al. [66].

strain rates. Transmitted light optical microscopy showed that under slow strain rate there was considerable crack tip blunting implying that significant shear flow must have taken place during deformation. Multiple craze-like bands[5] were also found by Zhang [49] in iPP/$CaCO_3$ nanocomposite double notch four-point bend specimens (see Fig. 11). There are few craze-like bands in the unfilled iPP (Fig. 11a), but in the nanocomposite containing 15% wt fraction of $CaCO_3$ particles (Izod impact energy about twice that of iPP) there are many more (Fig. 11b) and when 1.5% PN modifier (Izod impact energy about thrice that of iPP) was added there were even more (Fig. 11c). Obviously the β-phase affects the crazing behaviour. Labour et al. [50] suggest that the lower yield strength of the β-phase promotes early crazing and the higher density of tie molecules in the β spherulites provides stiffer fibrils. These observations are in keeping with the mechanical model of multiple crazing discussed above. Aboulfaraj et al. [51] have performed in situ tests on iPP under SEM and have come to similar conclusions that crazes are more easily initiated in β spherulites, but are more difficult to propagate. These observations again suggest that multiple crazes are more likely for higher β-phase fractions. All this evidence suggests that in iPP nanocomposites the toughness depends upon the presence of the β-phase as well as nanoparticles.

Although Zerbajad et al. [66] observed craze-like bands in impact iPP/$CaCO_3$ specimens, Zuiderduin et al. [36] apparently did not. They argue that if the adhesion between the particles and the matrix is low and debonding occurs early, then crazing is suppressed and shear yielding occurs. Since the presence of voided particles leads to higher normal stresses at the voids, this argument for the suppression of crazing cannot be accepted, but the SEM micrographs of cross sections near the fracture surface show highly elongated voids (see Fig. 12) do not seem to have localized into the dilatational bands observed by Zerbajad et al. [66]. The

[5] Since no SEM micrographs are available, it is impossible to tell whether these are true crazes or dilatational bands.

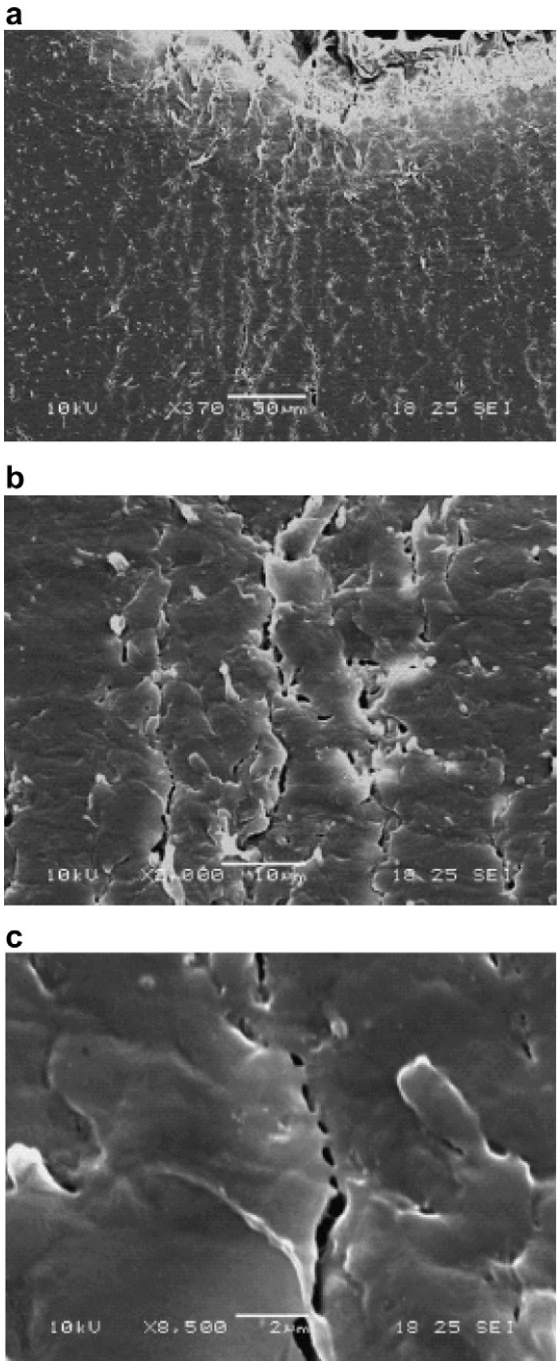

Fig. 10. SEM micrographs of polished surface of a 3-point bend specimen: (a) initiation of dilatational bands in front of the notch tip; (b) close up of (a); (c) dilatational band propagating near the notch; from Zebarjad et al. [66].

ligaments between the voids shown in (Fig. 12) are highly elongated, but presumably there was no strain softening or the deformation would have become localized.

Lamellae orientation has a large effect on deformation and fracture of semicrystalline polymers. When specimens are annealed the lamellae are organized to form spherulites, but in injection moulded specimens that are only a few millimetres thick the lamellae are orientated normal to the machine direction (MD) except possibly

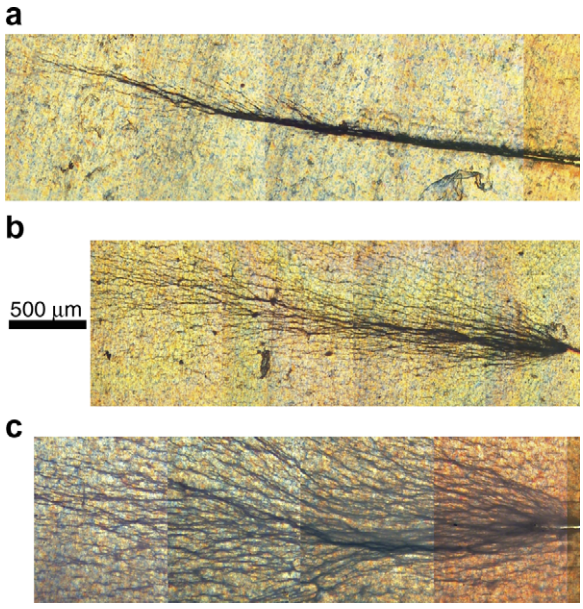

Fig. 11. Optical micrograph of multiple craze-like bands (a) iPP, (b) iPP + 15% wt $CaCO_3$, (c) iPP + wt15% $CaCO_3$ + 1.5% wt PN; from Zhang [49].

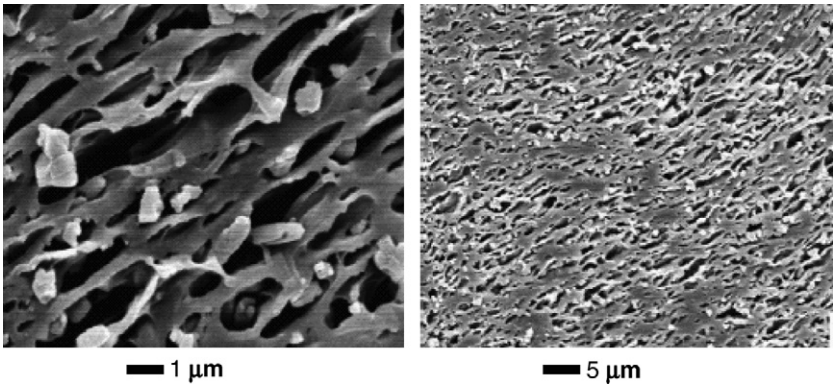

Fig. 12. SEM micrographs of sections normal to and 30 μm beneath the fracture surface of Izod specimens PP/CaCO 30% wt (From Zuiderduin et al. [36]).

in a narrow core region where the lamellae are arranged more isotropically. Zhou and Wilkes [68] have made TEM studies of the effect of orientation on the deformation of thin melt extruded polyethylene films where the lamellae are aligned normal to the MD. The results of Zhou and Wilkes [68] are shown schematically in Fig. 13. When the lamellae are stressed normal to their plane in the MD (Fig. 13a) they open up. The lamellae separation is accompanied by stress whitening and strain hardening. Initially deformation is by coarse slip causing the lamellae to fragment and craze. Interlamellar shear by chain slip is the dominant early deformation mechanism for loading at 45° to the MD (Fig. 13b) and takes place at a lower stress than either loading along or normal to the MD. The break up of the lamellae is essentially a cold drawing process taking place within the lamellae at almost constant stress. For deformation along the lamellae normal to the MD (Fig. 13c) there is little deformation within the lamellae by separation, shear or rotation, the yield is sharp and followed by localized break up of the lamellae and strain softening. Since most studies of semicrystalline polymer nanocomposites has been made on injection moulded specimens loaded in the MD one would expect, if the results of Corté et al. [52] are general, that there would be multiple crazing. Multiple crazing is observed for spherical

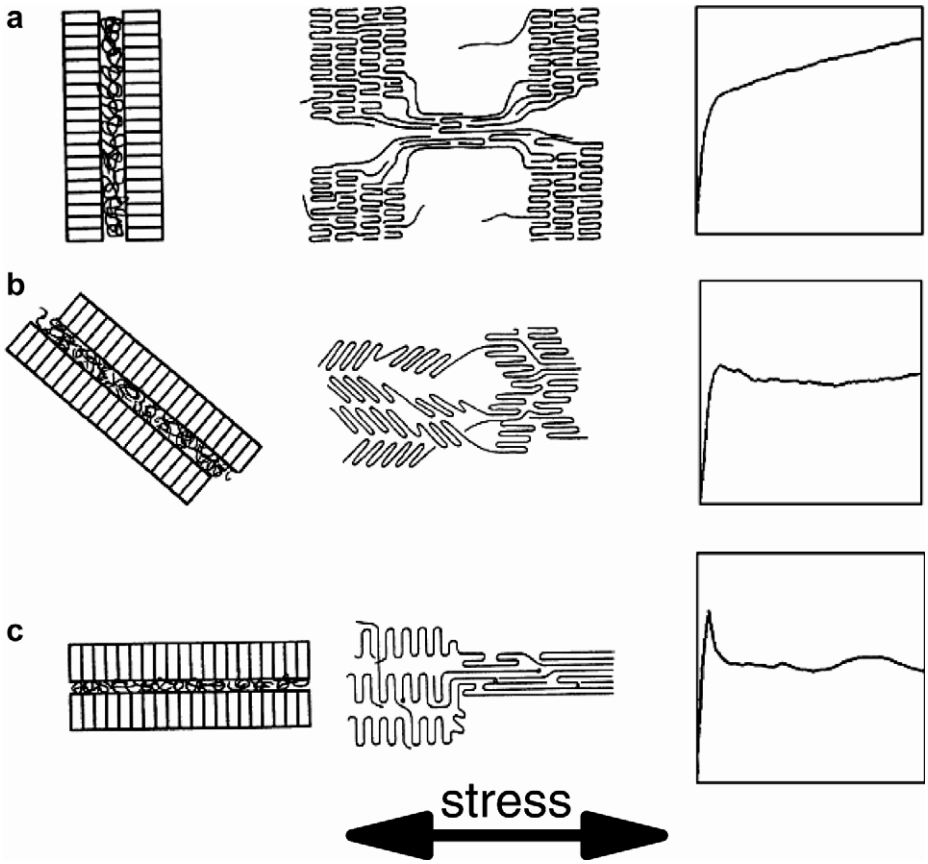

Fig. 13. Schematic illustration of deformation mechanism and stress–strain curve showing the effect of the lamellae orientation; after Zhou and Wilkes [68].

particle reinforced semicrystalline polymers, but not for those reinforced by nanoclay platelets. Possible reasons for the difference in behaviour between spherical and plate-like particles are discussed latter.

3. Semicrystalline polymers reinforced by nanoclay particles

Fully exfoliated clay has a layer thickness of about 1 nm and an aspect ratio of between 100 and 1000. However, electrostatic forces strongly resist intercalation of polymers between the layers and full exfoliation is difficult. Successful clay nanocomposites depend on the surface modification of the hydrophilic surfaces by cation exchange to produce an organoclay that can be more easily exfoliated. The four main methods of producing semicrystalline polymer/clay nanocomposites are (a) in situ polymerization, (b) emulsion polymerization, (c) sol–gel templating and (d) melt compounding [43]. In this section the method of manufacture is by melt compounding followed by injection moulding unless noted otherwise. Injection moulding produces strong orientation of the nanoclay particles in the injection moulding direction [69].

Nylon 6 has been the most extensively studied matrix. There are two major crystalline phases, monoclinic α-phase and monoclinic or pseudo hexagonal γ-phase [71]. The α-phase consists of fully extended planar zigzag chains, in which adjacent anti-parallel chains are joined by the hydrogen bonds. It is the most stable crystalline phase, and is obtained by slowly cooling from the melt. The γ-phase is composed of pleated sheets of parallel chains joined by a hydrogen bond, it is less stable, but can be obtained by fast cooling from the melt [70]. Clay particles also promote the γ-phase [45]. The γ-phase has a higher ductility than the α-phase [71]. In the last few years melt compounding has been the most common processing method for nylon 6 clay nanocomposites.

Liu et al. [45] performed Izod impact tests on nylon 6/clay nanocomposites and found that the impact energy decreased slightly with the nanoclay content falling to about 88% of that of unfilled nylon 6 at a clay content of 19% by weight. Fornes et al. [43] studied nylon 6/clay nanocomposites with low (LW) medium (MW) and high (HW) molecular weight. A better exfoliation was achieved with the higher molecular weight nylon 6. Again the clay did not greatly affect the Izod impact; for a clay content of about 7% by weight the LW impact energy decreased to 89%, the MW impact energy was unchanged and the HW impact energy increased to 105% of the unfilled nylon 6. Cho and Paul [44] obtained very similar impact energies for a HW nylon 6 nanocomposite. He et al. [39] used 3-point bend specimens with clay contents up to 10% by weight to measure the plane strain fracture toughness, $K_{Ic,}$ which decreased from 5.4 MPa $\sqrt{m}$ for the unfilled nylon 6 to 1.5 MPa $\sqrt{m}$ for 10% (wt) clay. If energies are compared then that is a staggering reduction in energy absorbed of more than 90%. However, since the validity criterion for thickness was violated for clay contents of less than 5% (wt) clay, the fractures in the unfilled nylon 6 and 2.5% (wt) clay nanocomposites would not have been plane strain; valid plane strain tests would have given smaller values, but the reduction in toughness is still very significant. He et al. [39] reported the absence of basal peaks in PA6/clay nanocomposites suggesting that the clay platelets are widely spaced, but did remark that transmission optical microscopy showed that there were some clay clusters for weight contents of 5% and above which may have caused premature fracture and account for the very low toughness. X-ray diffraction (XRD) showed that the γ-phase was strongly enhanced by the clay particles, but the overall crystallinity decreased [39]. Avlar and Qiao [72] also show that the γ-phase is enhanced by the presence of clay particles. Since the γ-phase is known to be more ductile than the α-phase, it shows that the mechanical embrittlement effect of the nanoclay particles is even more intense.

Nylon 66 normally crystallizes into a triclinic α-phase; nanoclay particles promote crystallization into the γ-phase which has a pseudo hexagonal form [73]. Nair et al. [74] measured J_{Ic} for nylon 66/clay nanocomposites with clay contents from 1 to 15% (wt). The initiation toughness decreases very significantly with increase in clay content. There was considerable crack growth resistance. Yu et al. [75] measured the plane strain fracture toughness, K_{Ic}, for well exfoliated nylon 66/clay nanocomposites with clay contents up to 10% (wt). The specimens they used had 12.7×12.7 mm cross sections and, since nylon 66 is not as tough as nylon 6, these gave valid K_{Ic}, values. There was very considerable scatter in the results at all clay contents. The average plane strain fracture toughness did decrease with clay content, but the decrease was not dramatic.

Phang et al. [40] performed Izod tests on nylon 12/clay nanocomposites. Nylon 12 crystallizes into monoclinc γ-form and the nanoclay does not introduce another crystal form. The impact energy of a nanocomposite with 5% (wt) clay was about 80% that of the unfilled nylon 12.

For the clay particles to be compatible with polypropylene it needs to be modified by an anhydride, usually maleic anhydride (PP-MA) [42]. The unfilled PP-MA crystallizes into the α-form and, as with other particles, the clay promotes the γ-phase [76]. Chen et al. [41] report a dramatic increase in J_{Ic} from 4 kJ/m^2 for the unfilled PP-MA to about 17 kJ/m^2 for 2.5% (wt) clay, which drops dramatically to about 3.7 kJ/m^2 for clay content of 5% (wt). Such a dramatic increase in toughness is unbelievable and must be due to the interpretation of the data, since they report a more modest increase in tearing modulus, which depends upon the slope of the crack growth resistance curve, from about 130[6] for the unfilled PP-MA to about 250 at 2.5% (wt) clay content and decreases roughly linearly to 50 at 10% (wt) content. The obvious inconsistency of the fracture data illustrates the point made in the introduction, that not enough emphasis and care is placed on the characterization of the toughness. For clay contents less than 10% (wt) Chen et al. [42] report that the clay is intercalated and partially exfoliated; not surprisingly there were many agglomerated particles for higher clay contents. Ton-That et al. [77] and Bureau et al. [22] have studied the effect of grafting of low and high molecular PP with maleic anhydride and reinforcing with 2% (wt) of clay. The various PP/clay compounds studied are given in Table 1. In order to attempt to obtain better clay dispersion some nanocomposites were processed from precompounded PP/clay. Two methods of processing and characterising the toughness were used. Ton-That et al. [77] obtained the Izod impact energy from injection moulded specimens whereas Bureau et al. [22] injection moulded 3 mm thick plates which were subsequently compression moulded down to 1 mm thickness and performed EWF tests. The results of these tests are shown, normalized by the toughness

[6] The tearing modulus is non-dimensional.

Table 1
Description of PP/clay compounds studied by Ton-That et al. [76] and Bureau et al. [22]

Designation	Matrix description	Type of modified clay
PP	Montell 6100SM	–
PP/MA9k	Low molecular weight, grafting Epolene E43	–
PP/MA330k	High molecular weight, grafting Polybond 3150	–
PP/15A	Montell 6100SM	2 wt% Cloisite 15A
PP/15A/MA9k	Low molecular weight, grafting Epolene E43	2 wt% Cloisite 15A
PP/15A/MA330k	High molecular weight, grafting Polybond 3150	2 wt% Cloisite 15A
m(PP/15A)/MA330k	From master batch of PP and 10% clay	2 wt% Cloisite 15A
m(PP/30B)/MA330k	From master batch of PP and 10% clay	2 wt% Cloisite 30B

of PP, in Fig. 14. The first obvious observation is how the test method affects the apparent toughness. In specimens PP/15A, PP15A/MA9k, and PP/15A/MA330k whereas the Izod tests indicated slight toughening, the EWF tests indicated very significant embrittlement; only for the nanocomposites produced from the precompounded PP/clay (m(PP/15A)/MA330k and m(PP/15A)/MA330k) did the two tests give comparable results. May be the improved dispersion in the precompounded specimens is a factor, but the very different nature of the two tests must affect the rating. In any case the conclusions from the work of Ton-That et al. [77] and Bureau et al. [22] is that 2% (wt) of clay does not significantly improve the toughness of PP. Reichert et al. [78] have shown that amine treatment of synthetic clay (SOMASIF ME100) as well as the type of maleic anhydride-modified PP affects the toughness of the nanocomposite. By increasing the amine content from 0 to 26.3% (wt) the interlayer spacing of the clay could be increased from 0.95 nm to 1.98 nm.. Using the Izod impact test to characterize the toughness of the PP nanocomposite, Reichert et al. [78] showed that the best toughness could be achieved in non-grafted PP and a modified silicate with amine content from 7.2 to 23.5% (wt). The best toughness achieved was for 10% (wt) clay modified with 18.4% (wt) amine and had a toughness of 2.2 times that of PP, but the AFM images (see Fig. 15) show that the particles were not well exfoliated, have a very low aspect ratio and are probably behaving similar to spherical particles. Slight embrittlement was observed for all the maleic anhydride treated PP nanocomposites. In common with $CaCO_3$ reinforcement the behaviour of clay reinforced PP is more difficult to characterize than with nylon as a matrix. The effect of the particles on promoting the β-phase is probably a major reason. Unfortunately not all researchers report on the different crystalline phases that are present. However, PP is not significantly toughened by clay nanoparticles in general.

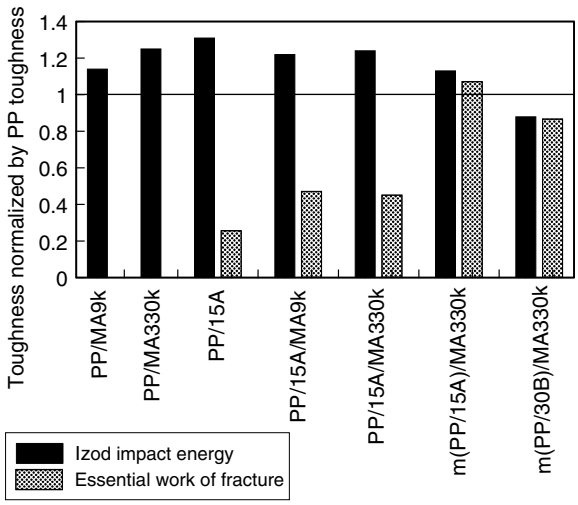

Fig. 14. Comparison of toughness of various PP and PP-MA nanocomposites; Data from [22,77].

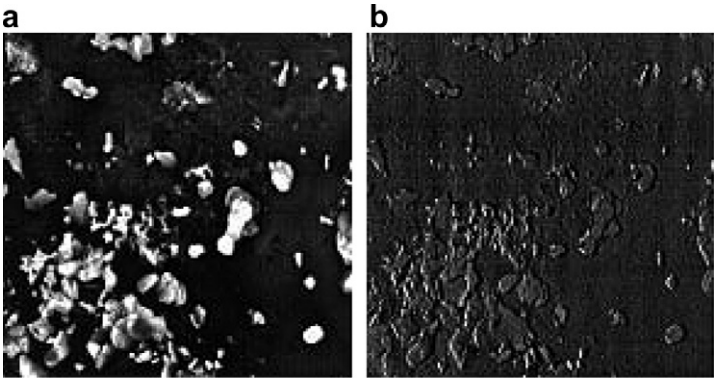

Fig. 15. AFM image: PP containing 5 wt% clay particles treated with 18.4% amine. This nanocomposite had twice the impact toughness of PP. View 20×20 μm, (a) phase mode, (b) height mode; from Reichert et al. [78].

3.1. Delamination or splitting of nanoclay particles

As with spherical particles, any toughening action depends upon the delamination of exfoliated or the splitting of intercalated particles at about the constrained yield stress. In situ TEM tensile tests have been made by Kim et al. [58] on thin films of nylon 12 reinforced by a synthetic layered silicate which show the silicate layers splitting to form voids (see Fig. 16). The energy released per unit volume by the delamination of particles is given by Eq. (7). For effective void formation at a nanoclay particle only one surface of the platelet needs to delaminate. If the particle splits it is the same fracture area. The particles in the Mori-Tanaka [60] model are oblate spheroids, but nanoclay particles are more nearly square plates with side l and thickness h, but the difference in effective particle surface area is not that significant. If the particle aspect ratio is high the total surface area per unit volume of nanocomposite is approximately $S = v_p/h$ if the particle is modelled as a square platelet, or $S = 1.5v_p/h$ if it is modelled as an oblate spheroid. Hence the condition for delamination, assuming a square platelet is given by

$$\Gamma_d \leqslant \frac{1}{2v_p}\left(\frac{\sigma_h^2 h}{E_m}\right)\left[\frac{E_m}{K_v} - \frac{E_m}{K_p}\right] \tag{14}$$

where here Γ_d is the energy of delamination of exfoliated particles or the fracture energy for splitting of intercalated particles. An alternative expression for the critical non-dimensional particle size, $\bar{d}_c$, defined as

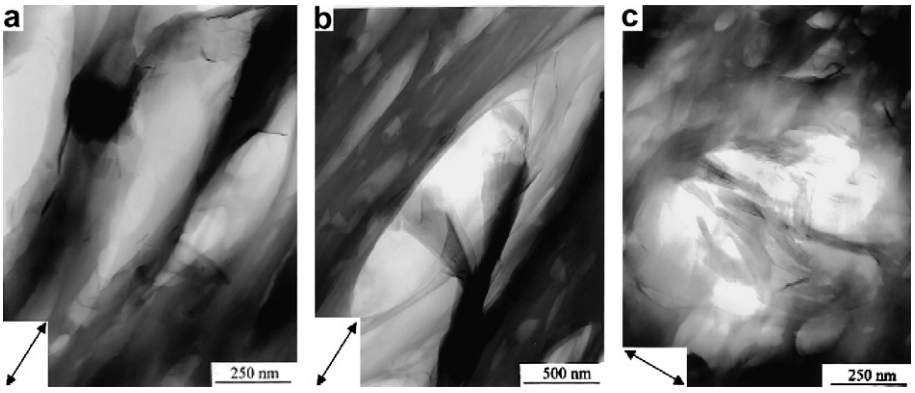

Fig. 16. Tensile direction is shown by the arrows (a) layered silicates stacked normal to applied stress (b) Oriented at an angle to the applied stress (c) orientated parallel to the applied stress; from Kim et al. [58].

$$\bar{d}_c = \frac{(l^2 h)^{1/3}}{(E\Gamma_d/\sigma_h^2)} \tag{15}$$

is

$$\bar{d}_c = 2\left(\frac{l}{h}\right)^{2/3} v_p \Big/ \left[\frac{E_m}{K_v} - \frac{E_m}{K_p}\right] \tag{16}$$

which provides a better insight into the role of particle size and aspect ratio, l/h. The bulk modulus of the clay particles and voids of the same size can be calculated for randomly orientated particles from Wang and Pyrz [61]. Fig. 17 gives the critical non-dimensional particle size as function of the volume fraction of the particles representative of fully exfoliated clay and three intercalated clay sheets. As with the spherical particles the volume fraction does not have a very significant effect on the critical particle size for delamination. For the same toughness, exfoliated particles are more difficult to delaminate than intercalated ones except at very small volume fractions. The specific energy release rates for nanoclay particles and spherical $CaCO_3$ particles are given in Table 2 based on nylon 6 assuming delamination occurs at constrained yield (uniaxial yield stress of 70 MPa enhanced by a factor of 3 for constraint). The higher aspect ratio and stiffer fully exfoliated nanoclay particle will not delaminate at the constrained yield stress unless the delamination or splitting energy is less than about 1 J/m^2. However, delamination of the lower aspect ratio intercalated particle is easier and comparable to the spherical $CaCO_3$ particle. For comparison the surface energy of montmorillonite is 0.205 J/m^2, $\Gamma_d = 2 \times 0.205 = 0.41$ J/m^2 [79]. Thus the splitting of nanoclay particles at about the constrained yield stress appears possible. Polypropylene has lower yield strength than nylon has significantly smaller specific maximum energy release rate and delamination at constrained yield would be corresponding more difficult.

3.2. The contribution to toughness of nanocomposites from the delamination of nanoclay particles

Because of the very large surface area to volume of clay nanoparticles the potential for toughening from just the delamination or splitting of the particles is much greater than for spherical particles which have

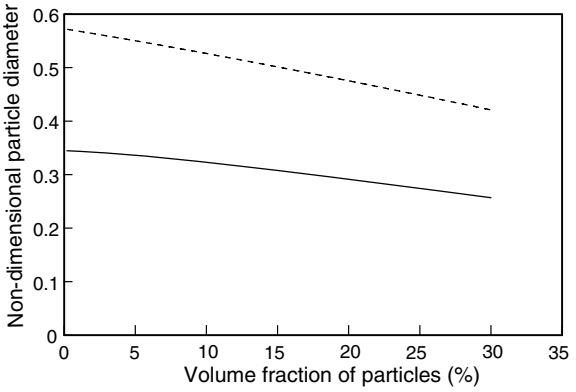

Fig. 17. Critical non-dimensional particle size for delamination —— $\frac{E_p}{E_m} = 95$, $\frac{l}{h} = 100$ Fully exfoliated, $h = 1$ nm – – – – $\frac{E_p}{E_m} = 21$, $\frac{l}{h} = 23$ Intercalated (three sheets), $h = 13$ nm.

Table 2
Maximum toughness for delamination or particle splitting in J/m^2 for properties representative of nylon/$CaCO_3$ and clay nanocomposites

Volume fraction of particles	Spherical $CaCO_3$ particle $d = 46$ nm	Fully exfoliated clay particle $h = 1$ nm	Three sheet intercalation particle $h = 8.6$ nm
1%	2.5 J/m^2	1.03 J/m^2	2.07 J/m^2
5%	2.6 J/m^2	1.17 J/m^2	2.14 J/m^2

(a) Spherical $CaCO_3$ particles $E_m = 2.6$ GPa, $\nu_m = 0.35$, $E_p = 26$ GPa, $\nu_m = 0.2$, (b) fully exfoliated platelets $E_m = 2.6$ GPa, $\nu_m = 0.35$, $E_p = 250$ GPa, $\nu_p = 0.2$, (c) three sheet intercalated clay platelets $E_m = 2.6$ GPa, $\nu_m = 0.35$, $E_p = 55$ GPa, $\nu_p = 0.2$.

the minimum surface area to volume ratio. The same argument is followed as in Section 2.3. If D is again the width on either side of the fracture plane where delamination or splitting is potentially possible, then the number of potential particles that can delaminate or split per unit area of fracture is given by

$$N = \frac{2v_p D}{l^2 h} \tag{17}$$

The potential contribution to the fracture toughness if all available particles delaminate or split Γ_{del}, is given by

$$\Gamma_{del} = N\Gamma_d l^2 = 2v_p\Gamma_d \frac{D}{h} \tag{18}$$

Substituting for D from Eq. (10) and using the definition of $\bar{d}_c$ from Eq. (15) we obtain

$$\frac{\Gamma_{del}}{\Gamma_c} \approx \frac{0.2v_p}{\bar{d}_c}\left(\frac{l}{h}\right)^{2/3} \tag{19}$$

From Fig. 17, $\bar{d}_c < 1$ and the ratio $\Gamma_{del}/\Gamma_c > 1$ which, of course, is impossible. The difference between the spherical particles and the nanoclay particles is the high surface area to volume of the particles. It has been assumed that the delamination or splitting of the particles does not affect the stress distribution. Such an assumption is reasonable if the particles are sparse, but cannot hold if the density is high. The unloading caused by delaminating or splitting particles unloads adjacent particles and the fraction of particles that delaminate or split must be low. Although the above approximate analysis is obviously inadequate, it does show that the delamination or splitting of nanoclay particles is a potentially a significant source of toughness which it is not for spherical particles.

3.3. Matrix energy absorbing mechanisms

As with semicrystalline polymer reinforced with spherical particles, shear yielding and craze-like bands are the mechanisms by which the matrix absorbs energy. Crazing was observed at the unfractured notch in double notch four point bend tests of nylon 6 nanoclay composites using transmitted optical microscopy under bright light and has been confirmed by TEM [39]. SEM observation of fracture surfaces in nylon 6 and PP by Gloaguen and Lefebvre [80] revealed fibrillation associated with clay particles. Similar observations were made for PP/nanoclay by Bureau et al. [22]. In the nylon 6/clay specimens of He et al. [39] multiple crazing was observed in the unfilled nylon 6 ($K_{Ic} = 5.4$ MPa $\sqrt{m}$), there was only very little crazing in the nylon 6 + 2.4% (wt) clay ($K_{Ic} = 3.4$ MPa $\sqrt{m}$) and just single crazes were observed for higher clay contents ($K_{Ic} \leqslant 2.1$ MPa $\sqrt{m}$) (see Fig. 18). Nanoclay particles seem to inhibit multiple crazing and this inhibition is a major source of embrittlement.

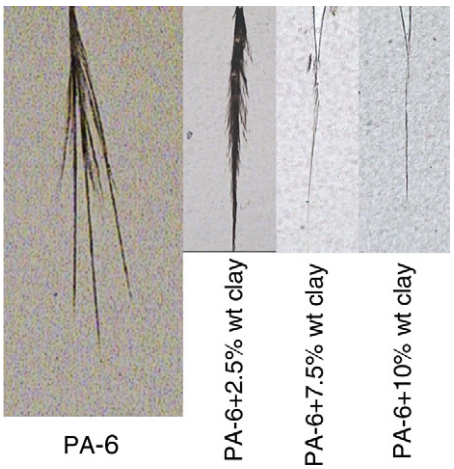

Fig. 18. Crazing in nylon 6/clay nanocomposite; from He et al. [39].

It seems unlikely that the suppression of multiple crazing in clay nanocomposites is caused by the structure or the chemistry of clay and more likely because of the large aspect ratio of the clay particles. Voids are necessary to initiate crazes, but the delamination of clay particles is only marginally more difficult than spherical particles and hence voids can form at clay particles almost as readily as at spherical particles and cannot be a significant factor in the difference in behaviour. A possible factor is the orientation of the clay particles. Most clay nanocomposites are produced by injection moulding and the clay is highly orientated in the injection moulding direction. The notches of the fracture specimens are almost invariably normal to the injection moulding direction. The orientation of clay particles in the usual injection moulded fracture specimen are shown schematically in Fig. 19a. Spherical particles on the other hand can have no orientation. Near the tip of the notch the state of stress is near hydrostatic, but the stress in the loading direction will be the larger. Assuming that the state of stress in the plane normal to the fracture plane is as shown in Fig. 19b where β is a little less than one. Under these conditions the stress at the equator and pole of a delaminated or voided spherical particle is given in Fig. 19c and for delaminated plate-like ellipsoidal particle of aspect ratio A, which

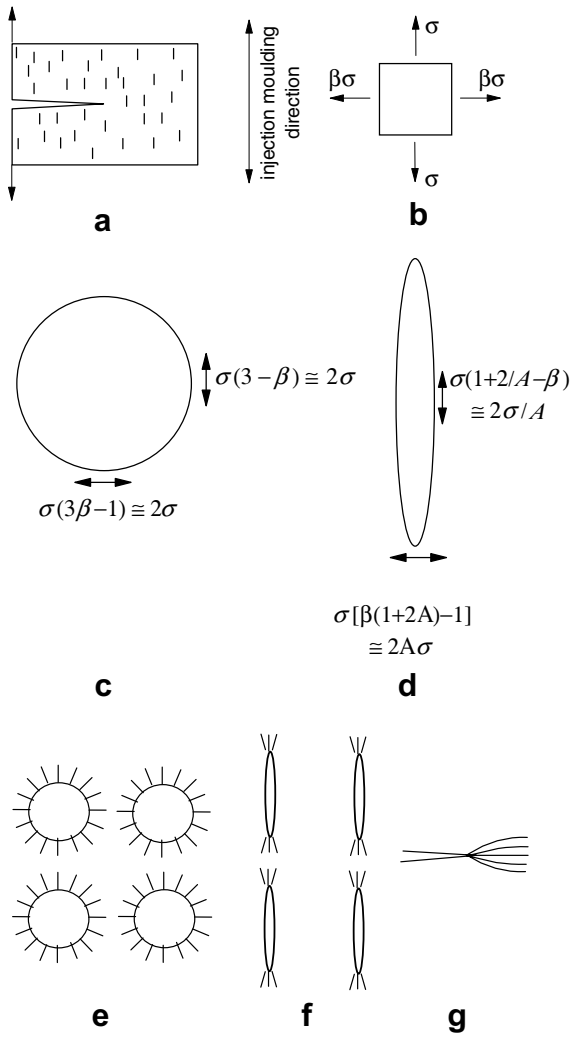

Fig. 19. (a) Schematic illustration of orientation of clay particles in an injection moulded nanocomposite. (b) Stresses near notch tip. (c) Stresses around spherical void (d) Stresses around ellipsoidal void aligned normal to fracture plane. (e) Possible craze initiation around spherical void. (f) Possible craze initiation around high aspect ratio plate-like void. (g) Schematic development of multiple crazes from a notch.

looks very like the split clay particles observed by Kim et al. [58] and shown in Fig. 16b and c, are as given in Fig. 19d [59]. The stress around a spherical void is almost uniform and crazes can initiate anywhere around the void (see Fig. 19e), whereas the stress at the equator of an ellipsoidal void is very much smaller than the stress at the pole (see Fig. 19f). For example if the aspect ratio50, the then stress at the equator is only about 0.04σ, whereas the stress at the pole is about 100σ. Thus crazes can be readily initiated at the pole, but not at the equator and hence the development of multiple crazes as shown schematically in Fig. 19g. Thus it is suggested that the orientation of the clay particles during injection moulding is in part responsible for the embrittlement of semicrystalline polymers by nanoclay particles. Experiments are planned to test this hypothesis by performing double cantilever beam tests with the notch in the direction of injection moulding as well as the more usual notch bend tests with the notch normal to the injection moulding direction.

An apparent contradiction to the above hypothesis comes from the fracture tests of Avlar and Qiao [72] on compression moulded nylon 6 clay where the orientation of the nanoclay particles would be expected to be more random. They obtained stable fracture for notched specimens of unfilled and 1.7% wt clay filled nylon 6; the toughness was characterised by the total work of fracture. For both the air cooled and quenched specimens they observed that the clay embrittled the specimens. Unfortunately no details of the crazing are provided. One would assume that clay particles orientated in the direction of the fracture plane would provide ready initiation sites for crazes. However, if a craze initiated at a favourably orientated nanoclay particle propagates it must, in a short distance, meet an unfavourably orientated particle which would cause unloading of the craze and perhaps its arrest. Only further experiments will determine whether this hypothesis of one of the reasons for the lack of multiple crazes and embrittlement in semicrystalline polymers is correct.

4. Conclusions

Although it is the functional properties of nanocomposites that are of prime interest their full potential will not be achieved unless their mechanical properties, especially fracture resistance, are optimised. There are many complex effects, chemical, physical and mechanical that control the fracture mechanisms and toughness. The optimum nanocomposite can only be obtained from a clear understanding of all the factors, trial and error is unlikely to succeed. One of the first problems is to ensure that the fracture toughness is well characterised. This review has been difficult partly because of the wide variety of fracture tests that have been used some of which have been inappropriate. It would be useful if the polymer nanocomposite community in cooperation with the fracture community could agree on the fracture characterization method for the various classes of polymer nanocomposite, especially the more ductile semicrystalline polymer nanocomposites.

From a mechanical point of view there are two main potential sources of toughness in semicrystalline polymer nanocomposites: delamination or splitting of particles and matrix deformation where the major energy absorbing mechanism is the formation of multiple craze-like bands, shear yielding does not seem to be as important. Spherical and plate-like particles appear to behave differently and toughening with spherical particles is easier than with plate-like particles. Hard particles must delaminate or split close to the constrained yield strength if multiple craze-like bands are to be initiated by the stress concentrations around voids. However, there does not seem to be a large difference between the delamination behaviour of spherical and plate-like particles. The delamination of particles depends primarily on the particle size, becoming more difficult as the particle gets smaller, with the volume fraction of the particles having little effect. Emphasis seems to be placed on improving the bonding of nanoclay to the polymer. Early delamination will certainly decrease the stiffness of a nanocomposite, but late delamination will embrittle it.

The energy absorbed in delamination is a potential source of toughening. For spherical particles it appears unlikely that this source of toughness can contribute more than about 10% of the toughness of the composite. However, a simple model shows that delamination or splitting of nanoclay particles could be a very significant source of toughness and a more exact study of the mechanics should be made.

Matrix deformation is the major source of toughness in semicrystalline polymer nanocomposites. The role of the interparticle ligament in promoting shear yielding or multiple crazing is somewhat unclear. Doubt has been thrown on the idea that the lamellar crystallites orientate themselves normal to the particles surface over a characteristic length and that toughening occurs if the interparticle distance is less than twice this characteristic distance. More work is needed to clarify the situation.

One important question to answer is why nanoclay particles do not usually significantly toughen semicrystalline polymers and very often produce very significant embrittlement? This question was the motivation for the present paper. Unfortunately we have not been able to give a really satisfying answer. We have suggested that it may be because of the orientation of the clay particles during injection moulding produces an unfavourable stress distribution for the initiation of crazes. In the only case where clay particles have caused a significant increase in toughness [78], the particles are not well exfoliated and have near spherical shape at the very least this case does not contradict the hypothesis advanced in this paper. Most fracture experiments have used injection moulded specimens, but in those few cases where compression moulding has been used, where the clay particles are not orientated, there is also embrittlement. However, it is believed that the answer is mechanical and probably lies in the high aspect ratio of the clay particle, especially since the crystal phases promoted by the particles are more ductile than those in the unfilled polymer.

Although in a sense this review has failed in that it has not given a clear and authoritative explanation of the fracture mechanisms and fracture toughness of semicrystalline polymer nanocomposites, it will have succeeded partially if it leads to more detailed study of the mechanics.

Acknowledgement

Dr. Chaobin He is warmly thanked for his many and helpful discussions on the fracture of semicrystalline polymer nanocomposites.

References

[1] Tjong SC. Structural and mechanical properties of polymer nanocomposites. Mater Sci Engng R-Reports 2006;53(3–4):73–197.
[2] Lomakin SM, Zaikov GE. Flame-resistant polymer nanocomposites based on layered silicates. Polymer Sci Series B 2005;47(1–2): 9–21.
[3] Kim JK, Hu CG, Woo RSC, Sham M-L. Moisture barrier characteristics of organoclay-epoxy nanocomposites. Comp Sci Tech 2005;65(5):805–13.
[4] Zhang Z, Yang JL, Friedrich K. Creep resistant polymeric nanocomposites. Polymer 2004;45(10):3481–5.
[5] Wetzel B, Haupert F, Friedrich K, Zhang MQ, Rong MZ. Impact and wear resistance of polymer nanocomposites at low filler content. Polymer Engng Sci 2002;42(9):1919–27.
[6] Sheng N, Boyce MC, Parks DM, Rutledge GC, Abes JI, Cohen RE. Multiscale micromechanical modeling of polymer/clay nanocomposites and the effective clay particle. Polymer 2004;45(2):487–506.
[7] Kinloch AJ, Mohammed RD, Taylor AC, Eger C, Sprenger S. The effect of silica nano particles and rubber particles on the toughness of multiphase thermosetting epoxy polymers. J Mater Sci 2005;45(18):5083–6.
[8] Ma C-CM, Chen Y-J, Kuan H-C. Polystyrene nanocomposite materials – Preparation, mechanical, electrical and thermal properties, and morphology. J Appl Poly Sci 2006;100(1):508–15.
[9] ISO-13586. Plastics – Determination of Fracture Toughness (GIc and KIc) – Linear Elastic Fracture Mechanics (LEFM) Approach. Geneva: ISO, 2000.
[10] Williams JG. Kc and Gc at slow speeds for polymers. In: Moore DR, Pavan A, Williams JG, editors. Fracture mechanics testing for polymers: ESIS pub 28. Amsterdam: Elsevier; 2001. p. 11–26.
[11] Hale GE, Ramsteiner F. *J*-fracture toughness of polymers at slow speed. In: Moore DR, Pavan A, Williams JG, editors. Fracture mechanics testing for polymers: ESIS pub 28. Amsterdam: Elsevier; 2001. p. 23–158.
[12] Dodds RH, Shih CF, Anderson TL. Continuum and micromechanics treatment of constraint in fracture. Int J Fract 1993;64(2): 101–33.
[13] Uribe-Arochaa P, Mehlerb I, Puskasc Altsta V. Effect of sample thickness on the mechanical properties of injection molded polyamide-6 and polyamide-6 clay nanocomposites. Polymer 2003;44(8):2441–6.
[14] Wilbrink MWL, Argon AS, Cohen RE, Weinburg M. Toughenability of nylon-6 with CaCO3 filler particles: new findings and general principles. Polymer 2001;42(25):10155–80.
[15] Joyce JA, Link RE. Effects of constraint on upper shelf fracture toughness. In: Reuter WG, Underwood JH, Newman JC, editors. Fracture mechanics: 26th volume. Philadelphia: American Society for Testing and Materials; 1995. p. 142–63.
[16] Xia L, Shih CF, Hutchinson JW. A computational approach to ductile crack growth under large scale yielding. J Mech Phys Solids 1995;43(3):389–413.
[17] Xia L, Shih CF. Ductile crack growth – I. A numerical study using computational cells with microscopically based length scales. J Mech Phys Solids 1995;43(3):233–59.
[18] Paris PC, Tada H, Zahoor A, Ernst H. The theory of instability of the tearing mode of elastic–plastic crack growth. In: Landes JD, Begley A, Clarke GA, editors. Elastic–plastic fracture, ASTM STP 668. Philadelphia: American Society for Testing and Materials; 1979. p. 5–36.

[19] Lach R, Schneider K, Weidisch R, Janke A, Knoll K. Application of the essential work of fracture concept to nanostructured polymer materials. Eur Poly J 2005;41(2):383–92.
[20] Qiao Y, Avlar S, Chakravarthula SS. Essential fracture work of nylon 6-silicate nanocomposites. J Appl Poly Sci 2005;95(4):815–9.
[21] Okada O, Keskkula H, Paul DR. Fracture toughness of nylon-6 blends with maleated rubbers. J Poly Sci Part B: Poly Phys 2004; 42(9):1739–58.
[22] Bureau MN, Perrin-Sarazin F, Ton-That M-T. Polyolefin nanocomposites: essential work of fracture analysis. Poly Engng Sci 2004;44(6):1142–51.
[23] Cotterell B, Reddel JK. The essential work of plane stress fracture. Int J Fract 1977;13(3):267–77.
[24] Mai YW, Cotterell B. On the essential work of ductile fracture in polymers. Int J Fract 1986;32920:05–126.
[25] Clutton E. Essential work of fracture. In: Moore DR, Pavan A, Williams JG, editors. Fracture mechanics testing for polymers: ESIS pub. 28. Amsterdam: Elsevier; 2001. p. 177–95.
[26] Wu JS, Mai YW. The essential fracture work concept for toughness measurement of ductile polymers. Poly Engng Sci 1996;36(18): 2275–88.
[27] Luna P, Bernal C, Cisilino A, Frontini P, Cotterell B, Mai YW. The application of the essential work of fracture methodology to the plane strain fracture of ABS 3-point bend specimens. Polymer 2003;44(5):145–1150.
[28] Wu JS, Mai YW, Cotterell B. Fracture-toughness and fracture mechanisms of PBT/ PC/IM blend Part1. Fracture properties. J Mater Sci 1993;289120:3373–84.
[29] Cotterell B, Pardoen T, Atkins AG. Measuring toughness and the cohesive stress-displacement relationship by the essential work of fracture concept. Engng Fract Mech 2005;72(6):827–48.
[30] Bucknall CB. Toughened plastics. London: Applied Science; 1977.
[31] Wu S. Phase structure and adhesion in polymer blends: a criterion for rubber toughening. Polymer 1985;26(12):1855–63.
[32] Wu S. A generalized criterion for rubber toughening: a critical matrix ligament thickness. J Appl Poly Sci 1988;35(2):549–61.
[33] Kim G-M, Michler GH. Micromechanical deformation processes in toughened and particle filled semicrystalline polymers. Part 2: Model representation for micromechanical deformation processes. Polymer 1998;39(22):5699–703.
[34] Chan C-M, Wu J, Li J-X, Cheung Y-K. Polypropylene/calcium carbonate nanocomposites. Polymer 2002;43(10):2981–92.
[35] Thio YS, Argon AS, Cohen RE, Weinberg M. Toughening of isotactic polypropylene with CaCO3 particles. Polymer 2002;43(11): 3661–74.
[36] Zuiderduin WCJ, Westzaan C, Huétink J, Gaymans RJ. Toughening of polypropylene with calcium carbonate particles. Polymer 2003;44(1):261–75.
[37] Zhang Q-X, Yua Z-Z, Xie X-L, Mai YW. Crystallization and impact energy of polypropylene/CaCO3 nanocomposites with nonionic modifier. Polymer 2004;45(17):5985–94.
[38] Bartczak Z, Argon AS, Cohen RE, Weinberg M. Toughness mechanism in semi-crystalline polymer blends:II. High-density polyethylene toughened with calcium carbonate filler particles. Polymer 1999;40(9):2347–65.
[39] He C, Liu T, Tjiu WC, Sue H-J, Yee AF. Deformation and fracture mechanisms in polyamide 6/organoclay nanocomposites. Macromolecules, Submitted for publication.
[40] Phang IY, Liu T, Mohamed A, Pramoda KP, Chen L, Shen L, et al. Morphology, thermal and mechanical properties of nylon 12/ organoclay nanocomposites prepared by melt compounding. Poly Int 2005;54(2):456–64.
[41] Chen L, Wong S-C, Liu T, Lu X, He C. Deformation mechanisms of nanoclay-reinforced maleic anhydride-modified polypropylene. J Poly Sci: Part B: Poly Phys 2004;42(14):2759–68.
[42] Chen L, Wong S-C, Pisharath S. Fracture properties of nanoclay-filled polypropylene. J Appl Poly Sci 2003;88(12):3298–305.
[43] Fornes TD, Yoon PJ, Keskkula H, Paul DR. Nylon 6 nanocomposites: the effect of molecular weight. Polymer 2001;42(25):9929–40.
[44] Cho JW, Paul DR. Nylon 6 nanocomposites by melt compounding. Polymer 2001;42(3):1083–94.
[45] Liu L, Qi Z, Zhu X. Studies on nylon 6/clay nanocomposites by the melt-intercalation process. J Appl Poly Sci 1999;71(7):1133–8.
[46] Muratoglu OK, Argon AS, Cohen RE, Weinberg M. Toughening mechanism of rubber-modified polyamides. Polymer 1995;36(5): 921–0930.
[47] Bartczak Z, Argon AS, Cohen RE, Weinberg M. Toughness mechanism in semi-crystalline polymer blends: I. High-density polyethylene toughened with rubbers. Polymer 1999;40(9):2331–46.
[48] Lazzeri A, Zebarjad SM, Pracella M, Cavalier K, Rosa R. Filler toughening of plastics. Part 1 – The effect of surface interactions on physico-mechanical properties and rheological behaviour of ultrafine CaCO3/HDPE nanocomposites. Polymer 2005;46(3):827–44.
[49] Zhang Q-X. Private communication.
[50] Labour T, Vigier G, Séguéla R, Gauthier C, Orange G, Bomal Y. Influence of the β-crystalline phase on the mechanical properties of unfilled and calcium carbonate-filled polypropylene: ductile cracking and impact behaviour. J Poly Sci Part B: Poly Phys 2002;40(1): 31–42.
[51] Aboulfaraj M, G'Sell C, Ulrich B, Dahoun A. In situ observation of the plastic deformation of polypropylene spherulites under uniaxial tension and simple shear in the scanning electron microscope. Polymer 1995;36(4):731–42.
[52] Corté L, Beaume F, Leiblera L. Crystalline organization and toughening: example of polyamide-12. Polymer 2005;46(8):2748–57.
[53] Muratoglu OK, Argon AS, Cohen RE. Crystalline morphology of polyamide-6 near planar surfaces. Polymer 1995;36(11):2134–52.
[54] Bartczak Z, Argon AS, Cohen RE, Kowaleski T. The morphology and orientation of polyethylene in films of sub-micron thickness crystallized in contact with calcite and rubber substrates. Polymer 1999;40(9):2367–80.
[55] Stern T, Marom G, Wachtel E. Origin morphology and crystallogrsaphy of transcrystallinity in polyethylene-based single polymer composites. Composites Part A 1997;28(3):437–44.

[56] Stern T, Wachtel E, Marom G. Epitaxy and lamellar twisting in transcrystalline polyethylene. J Poly Sci: Part B: Poly Phys 1997; 35(15):2429–33.
[57] Klein N, Marom G, Wachtel E. Microstructure of nylon 66 transcrystalline layers in carbon and aramid fibre reinforced composites. Polymer 1996;37(24):5493–8.
[58] Kim G-M, Lee D-H, Hoffmann B, Kressler J, Stöppelmann G. Influence of nanofillers on the deformation process in layered silicate/polyamide-12 nanocomposites. Polymer 2001;42(3):1095–100.
[59] Timoshenko S, Goodier JN. Theory of elasticity. New York: McGraw-Hill; 1951.
[60] Mori T, Tanaka K. Average stress in matrix and average elastic energy of materials with misfitting inclusions. Acta Metall 1973; 21(5):571–4.
[61] Wang J, Pyrz R. Prediction of the overall moduli of layered silicate-reinforced nanocomposites – part I: basic theory and formulas. Comp Sci Tech 2004;64(7-8):925–34.
[62] Putánszky B. In: Karger-Kocsis J, editor. Polypropylene: structure, blends and composites. London: Chapman Hall; 1995 (Chapter 1).
[63] Hill R. The mathematical theory of plasticity. Oxford: Clarendon Press; 1950.
[64] Lazzeri A, Bucknall CB. Applications of a dilatational yielding model to rubber toughened polymers. Polymer 1996;35(15):2895–902.
[65] Estevez R, Tijssens MGA, Van der Giessen E. Modeling of the competition between shear yielding and crazing in glassy polymers. J Mech Phys Solids 2000;48(12):2585–617.
[66] Zerbarjad SM, Lazzeri A, Bagheri B, Seyed Reihani SM, Founcji M. Fracture mechanism under dynamic loading of elastomer-modified polypropylene. Mater Lett 2003;57(18):2733–41.
[67] Fasce LA, Frontini PM, Wong S-C, Mai YW. Polypropylene modified with elastomeric metallocene-catalyzed polyolefin blends: fracture behavior and development of damage mechanisms. J Poly Sci Part B: Poly Phys 2004;42(6):1075–89.
[68] Zhou H, Wilkes GL. Orientation-dependent mechanical properties and deformation morphologies for uniaxially melt-extruded high-density polyethylene films having an initial stacked lamellar texture. J Mater Sci 1998;33(2):287–303.
[69] Usuki A, Hasegawa N, Kadoura H, Okamoto T. Three dimensional observation of structure and morphology in nylon 6-clay nanocomposites. Nano Lett 2001;1(5):271–2.
[70] Brucato V, Crippa G, Piccarolo S, Titomanlio G. Crystallization of polymer melts under fast cooling, 1. nucleated polyamide-6. Poly Engng Sci 1991;31(19):1411–6.
[71] Ito M, Mizuochi K, Kanamoto T. Effects of crystalline forms on the deformation of nylon 6. Polymer 1998;39(19):4593–8.
[72] Avlar S, Qiao Y. Effects of cooling rate on fracture resistance of nylon 6-silicate nanocomposites. Composites Part A 2005;36(3): 624–30.
[73] Liu X, Wu Q, Berglund LA. Polymorphism in polyamide 66/clay nanocomposites. Polymer 2002;43(18):4967–72.
[74] Nair SV, Goettler LA, Lysek BA. Toughness of nanoscale and multiscale polyamide-6,6 composites. Poly Engng Sci 2002;42(9): 1872–82.
[75] Yu Z-Z, Yan C, Yang M, Mai YW. Mechanical and dynamic mechanical properties of nylon 66/montmorillonite nanocomposites fabricated by melt compounding. Poly Int 2004;53(8):1093–8.
[76] Nam PH, Maiti P, Okamoto M, Kotaka T, Hasegawa N, Usuki A. A hierarchical structure and properties of intercalated polypropylene/clay nanocomposites. Polymer 2001;42:9633–40.
[77] Ton-That M-T, Perrin-Sarazin F, Cole KC, Bureau MN, Denault J. Polyolefin nanocomposites: formulation and development. Poly Engng Sci 2004;44(7):1212–9.
[78] Reichert P, Nitz H, Klinke S, Brandsch R, Thomann R, Mülhaupt R. Poly(propylene)/organoclay nanocomposite formation: Influence of compatibilizer functionality and organoclay modification. Macromol Mater Engng 2000;275(1):8–17.
[79] Helmy AK, Ferreiro EA, de Bussetti SG. The surface energy of montmorillonite. J Colloid Interf Sci 2003;268(1):263–5.
[80] Gloaguen JM, Lefebvre JM. Plastic deformation behaviour of thermoplastic/clay nanocomposites. Polymer 2001;42(13):5841–7.